scientific reports

Check for updates

OPEN

Next-generation orange-to-far-red photoconvertible fluorescent protein for single-molecule microscopy and protein dynamic tracking

Oksana M. Subach[1], Fakorede Olumayowa[2,3,4], Muyuan Tang[3], Yu Qiao[3], Yongdeng Zhang[2,3], Anna V. Vlaskina[1], Alena Y. Nikolaeva[1], Alexey S. Kononikhin[5], Yulia K. Agapova[1], Anatolii Belousov[6], Valentin Borshchevskiy[6], Valeriya R. Samygina[1], Maxim M. Perfilov[7], Alexander S. Mishin[7], Kiryl D. Piatkevich[2,3,4] & Fedor V. Subach[1]✉

The PSmOrange and PSmOrange2 fluorescent proteins undergo irreversible photoconversion from the orange to far-red form under blue light, which makes them probes of choice for protein tracking and single-molecule super-resolution imaging. However, both proteins exhibit noticeable photoconversion under 550–570 nm light used for excitation of their orange form, which complicates applications of these photoconvertible FPs in cell imaging experiments. Here, we report the next-generation PSmOrange variant, called PSmOrange3, which is characterized by minimal photoconversion under 550–570 nm light and high photoconversion contrast. PSmOrange3 undergoes efficient photoconversion from the orange (Ex/Em at 550 nm/564 nm) to far-red form (Ex/Em at 614 nm/655 nm) with 430–470 nm violet-blue light of moderate power density (3-180 mW/mm^2) in a native cellular environment. The molecular brightness of orange and far-red forms of PSmOrange3 was 1.2- and 1.4-fold brighter than that of PSmOrange2. In addition, PSmOrange3 had a substantially higher photostability of the orange form but a little less photostability of the far-red form. We solved the crystal structure of PSmOrange3 at a 2.8 Å resolution, which confirmed its monomeric state and revealed the role of the introduced mutations in the properties of PSmOrange3. Using mass spectrometry we revealed the chemical structure of the PSmOrange3 chromophore before and after photoconversion. PSmOrange3 was properly localized with different protein fusions and photoconverted from the orange to far-red state inside live and fixed mammalian cells without exogenously supplied oxidants. Among all proteins of the PSmOrange series, both forms of PSmOrange3 were the brightest in the reducing environment of the mitochondrial lumen. PSmOrange3 photoconverted efficiently with blue light and almost did not photoconvert with green light, which allows investigators to excite its orange form and photoconvert it to the far-red form with different light. We demonstrated the applicability of PSmOrange3 for photoactivated localization microscopy (PALM) of tubulin microtubules using 488-nm photoconversion, achieving mean localization precision per single-molecule event of 24.6 and 23.3 nm in fixed and live mammalian cells, respectively. We believe that PSmOrange3 can represent a suitable alternative to the PSmOrange and PSmOrange2 proteins and will be a valuable addition to the repertoire of available photoconvertible fluorescent proteins.

Keywords Genetically encoded orange-to-far-red photoconvertible fluorescent proteins, Protein engineering, Fluorescence imaging, Photoconversion, Fluorescent protein

[1]Complex of NBICS Technologies, National Research Center "Kurchatov Institute", 123182 Moscow, Russia. [2]School of Life Sciences, Westlake University, Hangzhou, Zhejiang, China. [3]Westlake Laboratory of Life Sciences and Biomedicine, Hangzhou, Zhejiang, China. [4]Institute of Basic Medical Sciences, Westlake Institute for Advanced Study, Hangzhou, Zhejiang, China. [5]Project Center of Omics Technologies and Advanced Mass Spectrometry, 121205 Moscow, Russia. [6]Moscow Institute of Physics and Technology, Dolgoprudny 141701, Russia. [7]Shemyakin-Ovchinnikov Institute of Bioorganic Chemistry, Russian Academy of Sciences, Moscow 117997, Russia. ✉email: subach_fv@nrcki.ru

Abbreviations

PCFPs	PhotoconvertiblePhotoconvertible fluorescent proteins
FPLC	Fast protein liquid chromatography
FP	Fluorescent protein
PBS	Phosphate Buffered Saline
PFA	Paraformaldehyde
QY	Quantum yield
PALM	Photoactivated localization microscopy
SD	Standard deviation
LED	Light emiting diode

Photoconvertible fluorescent proteins (PCFPs) undergo an irreversible transition from one fluorescent state to a red-shifted state upon exposure to ultraviolet, violet, or blue light. The majority of PCFPs, such as Dendra2[1], mEos2[2], mEos3.2[3], mKikGR[4], mMaple[5], mClavGR2[6], and their derivatives change their fluorescence from green to red with ultraviolet or violet light illumination (365–405 nm). There is also PSCFP2 that changes fluorescence from blue to green with ultraviolet or violet light illumination[1].

A pair of orange-to-far-red PCFPs, PSmOrange[7] and PSmOrange2 [8], which are photoconverted with blue-green light, represent a unique class of PCFPs. The structural determinants of the orange and far-red forms, which are markedly distinct from those of other PCFPs, were revealed by X-ray crystallography[9] and mass spectrometry[7]. The orange forms of PSmOrange and PSmOrange2 consisted of a three-aromatic-ring system of p-hydroxyphenyl, imidazolinone, and 2-hydroxy-dihydrooxazole[9]. The far-red fluorescence observed in the photoconverted PSmOrange was attributed to the formation of an N-acylimine group, which extended the π-conjugated system of the chromophore with a co-planar carbon-oxygen double bond[7]. PSmOrange was suitable for protein tracking under a conventional fluorescent microscope and for single-molecule super-resolution imaging in the far-red range of the visible spectrum. Furthermore, PSmOrange could be photoconverted subcutaneously in live mice[7]. PSmOrange2, owing to its more efficient photoconversion properties compared to PSmOrange, could be photoconverted with standard two-photon lasers and with violet one-photon light through green fluorescent donors and Förster resonance energy transfer (FRET)[8]. Therefore, both orange-to-far-red PCFPs can be efficiently photoconverted using less phototoxic blue-green light.

Here, we report the development and characterization of the enhanced version of PSmOrange2, called PSmOrange3, which can undergo efficient photoconversion upon blue (455–490 nm) light illumination. Both fluorescent forms of the novel PCFP were brighter than those of the parental PSmOrange2. In addition, the orange form of PSmOrange3 was substantially more photostable than that of PSmOrange2, allowing for longer live cell imaging sessions. We determined the crystal structure of PSmOrange3 at 2.8 Å resolution and investigated the role of mutated amino acid residues in the chromophore environment. PSmOrange3 was accurately localized within live and fixed mammalian cells when fused with various structural proteins, including vimentin, keratin, and the microtubule-binding domain of ensconsin (EMTB), which are sensitive to the oligomeric state of a tagging fluorescent protein[10]. We also discovered that PSmOrange3, in contrast to PSmOrange and PSmOrange2, does not undergo photoconversion under illumination used for orange form excitation. In addition, we demonstrated the applicability of PSmOrange3 in the reducing environment of the mitochondrial lumen. Furthermore, we characterized the photoconversion of PSmOrange3 in mammalian cells and demonstrated its applicability for protein tracking and photoactivated localization microscopy using 488-nm photoconversion illumination.

Results and discussion

Development of PSmOrange3 photoconvertible fluorescent protein

To develop an enhanced PSmOrange variant with improved photoconversion contrast and far-red brightness under native physiological conditions, we employed directed molecular evolution using PSmOrange2 as a starting template[8]. Specifically, we conducted five sequential rounds of random mutagenesis followed by colony screening on Petri dishes to identify variants with the highest fluorescence ratio in the far-red channel (excitation: 620/60 nm, emission: 700/75 nm) before and after illumination with a 463/16 nm LED array (200 mW/cm^2, 30 min), without adding exogenous oxidants. After screening on colonies, the top 150–200 clones were selected and reassessed on bacterial streaks under identical screening conditions, and then the top 5–10 clones with the highest fluorescence in the far-red channel were selected for sequence analysis. For the subsequent round, we used only 1–3 top-performing clones that carried distinct amino acid mutations. The accumulated mutations after each round of evolution are summarized in Figure S1. As a result, we identified a final optimized variant, named PSmOrange3 (PSmOrange2/I29V/E32K/A44V/I65V/I161V/V177A/Y208F/M226K), which contains five amino acid mutations facing into the β-barrel and three mutations facing outward the β-barrel relative to its parental protein, PSmOrange2 (Fig. 1).

Characterization of the purified PSmOrange3 in solution

To characterize PSmOrange3 in solution, we measured absorption and fluorescence spectra and estimated the molecular brightness of the orange form of PSmOrange3 and the far-red form after photoconversion with an LED at 463/17 nm. The orange form had maxima of absorption/excitation/emission at 548/550/564 nm, respectively (Fig. 2a-b; Table 1). After photoconversion, we observed the appearance of the absorption peak with a maximum of 613 nm (Fig. 2a). The far-red form had excitation/emission maxima at 614/655 nm, respectively (Fig. 2b; Table 1). Molecular brightness of both forms of PSmOrange3 was 1.2- and 1.4-fold higher than that of PSmOrange2 (Table 1).

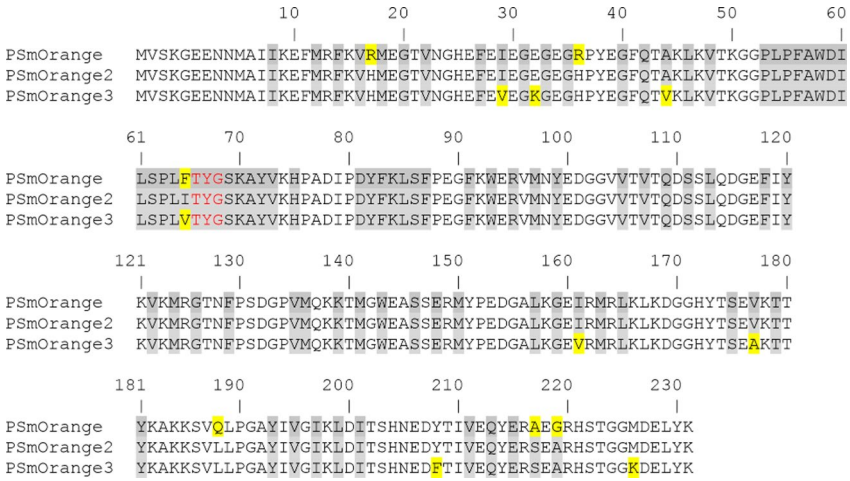

Fig. 1. Alignment of the amino acid sequences for the PSmOrange, PSmOrange2, and PSmOrange3. Residues from the fluorescent part buried in the β-barrel are highlighted with grey. Residues that form the chromophore are in red. Mutations in PSmOrange and PSmOrange3 related to PSmOrange2 are highlighted in yellow.

Next, we characterized biochemical and photochemical properties of PSmOrange3 compared to PSmOrange2. First, we checked pH stabilities of the orange and far-red forms at the pH range of 3.0–10.0 (Fig. 2c; Table 1). PSmOrange3 had a similar pK_a value for its orange form as PSmOrange2, and a 0.5-unit higher pK_a value for its far-red form. Consequently, the pH stabilities of PSmOrange3 and PSmOrange2 were comparable.

We further compared photostabilities of PSmOrange3 and PSmOrange2 under wide-field illumination. In contrast to PSmOrange2, the photobleaching curve for the PSmOrange3 orange form exhibits triphasic character with a rapid initial drop followed by a slower component (Fig. 2 d), which is likely related to the photochromic behavior similarly observed earlier for mApple, TagRFP-T, mRuby2, and mRuby3 red fluorescent proteins[13]. As a result, photobleaching half-time for the PSmOrange3 orange form was about 10-fold higher than for PSmOrange2 (Fig. 2 d; Table 1). Higher photostability of PSmOrange3 orange form is advantageous for prolonged fluorescence imaging in mammalian cells, for example, for dynamic tracking of some intracellular proteins or organelles. Photobleaching half-time for the PSmOrange3 far-red form was 1.3-fold lower than for PSmOrange2 (Fig. 2e; Table 1). Notably, photobleaching rates became similar for both proteins in the far-red state when fluorescence dropped below 35%.

We also compared the photoconversion quantum yields for both forms of PSmOrange2 and PSmOrange3. In the case of orange forms, the photoconversion quantum yield for PSmOrange2 was 1.3-fold higher than for PSmOrange3 (Figure S2a). At the same time, photoconversion quantum yield for PSmOrange3 far-red form was 2.2-fold higher (Figure S2b). Therefore, the PSmOrange3 orange form has a lower photoconversion yield that is in accordance with its higher photostability. However, the transition of the orange form to the far-red form upon photoconversion was more efficient in the case of PSmOrange3 than for PSmOrange2, i.e. for every orange molecule that underwent photoconversion, more far-red molecules were formed for PSmOrange3.

The maturation half-time for PSmOrange3, measured at 37 °C using purified protein, was 12% faster than that for the parental PSmOrange2 (Fig. 2f; Table 1). According to FPLC, at 180 μM concentration, PSmOrange3 was monomeric in the solution (Fig. 2 h, g). Overall, PSmOrange3 outperformed parental protein in terms of molecular brightness of the orange and far-red forms and photostability of the orange form, while other biochemical parameters were comparable.

Structural characterization of PSmOrange3

To understand the impact of the introduced mutations on the properties of PSmOrange3, we determined its crystal structure using X-ray diffraction at a resolution of 2.8 Å and compared it to the PSmOrange2 structure (Fig. 3 and Table S1). The 3D protein structures of PSmOrange2 and PSmOrange3 were almost identical. Consistent with crystallographic data indicating that PSmOrange3 contains only one subunit per crystallographic unit, it behaved as a monomer in solution even at the high concentrations used for crystallization (Fig. 2 g, h). Like all other GFP-like FPs, the PSmOrange3 subunit featured a β-barrel structure with a central α-helix containing the ^{66}TYG^{68} chromophore (Fig. 3a). PSmOrange3 possessed a typical chromophore for orange FPs, comprising three rings: p-hydroxyphenyl, imidazolinone, and 2-hydroxy-dihydrooxazole (Fig. 3b). The chromophore in PSmOrange3 was in a cis-configuration and formed three direct hydrogen bonds (H-bonds) with S69, R95, and S146, along with five water-mediated H-bonds to L64, Q109, S111, E144, and L199 (depicted in Fig. 3c).

We suggested that the I65V mutation, located right before the first amino acid of the chromophore (T66), might be crucial for the efficient photoconversion of PSmOrange3 (Fig. 3 d, Figure S3). In the previous study, mass-spectrometry analysis of the photoconverted chromophore-containing peptide of PSmOrange facilitated the proposal of a photoconversion mechanism, which involved a cleavage of the polypeptide chain between the main chain carbonyl and Cα of F65, the amino acid before the chromophore[7]. The same mechanism of photoconversion involving a cleavage of the polypeptide chain between the main chain carbonyl and Cα of I65,

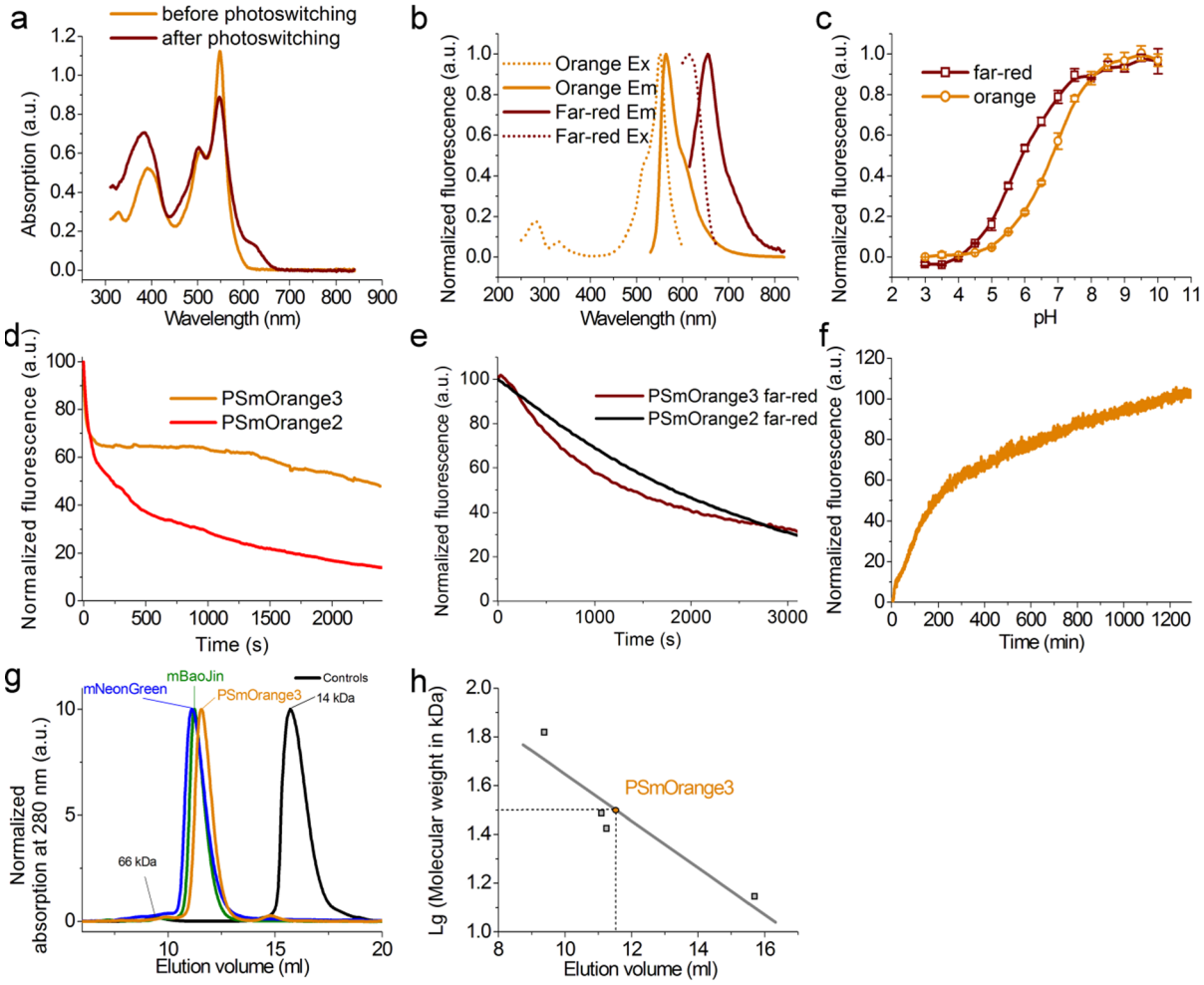

Fig. 2. In vitro properties of the purified PSmOrange3. (**a**) Absorption spectra for PSmOrange3 protein in PBS buffer at pH 7.40 before and after photoconversion with LED at 463/17 nm, 200 mW/cm^2 for 3 min. (**b**) Excitation and emission spectra for PSmOrange3 protein in PBS buffer at pH 7.40 before and after photoconversion with LED at 463/17 nm, 200 mW/cm^2 for 3 min. (**c**) Orange and far-red fluorescence intensity for PSmOrange3 as a function of pH. (**d**) Photobleaching of orange forms for PSmOrange2 and PSmOrange3 protein droplets in oil under continuous wide-field imaging using metal halide lamp with 550/25 nm light (53 mW/mm^2 light power density in the focus of the objective lens). (**e**) Photobleaching of far-red forms for PSmOrange2 and PSmOrange3 protein droplets in oil under continuous wide-field imaging using metal halide lamp with 620/60 nm light (0.56 mW/mm^2 light power density in the focus of the objective lens). (**c**–**e**) Three-six replicates were averaged for analysis. Error bars represent the standard deviations. (**f**) Maturation of PSmOrange3 in PBS buffer at pH 7.40. (**g**) Fast protein liquid chromatography (FPLC) of PSmOrange3 (180 μM) and molecular weight standards: BSA(66 kDa), mNeonGreen (31 kDa), mBaoJin (26.6 kDa), and lysozyme (14 kDa). (**h**) Calibration curve for FPLC for the calculation of molecular weight of PSmOrange3 (30.7 kDa - theoretical and 31.6 kDa – experimental).

the amino acid before the chromophore, was also previously suggested for PSmOrange2 [9]. We speculated that PSmOrange3 photoconversion was also accompanied by a break of the polypeptide chain between the main chain carbonyl and Cα of Val65. Perhaps this break could occur more easily in PSmOrange2 with Ile than in PSmOrange3 with Val in the position right before the chromophore, because we observed a greater decrease of the orange fluorescence upon photoconversion in mammalian cells (see results below). Therefore, we suggest that photoconversion of PSmOrange3 should also involve a break of the polypeptide chain between the main chain carbonyl and Cα of the valine residue upstream of the first amino acid of the chromophore.

The other introduced mutations may improve chromophore packing and protein folding. In addition to I65V, there are three other mutations in PSmOrange3, namely I29V, A44V, and I161V, that are close to the chromophore (Fig. 3d, Figure S3). The side chain of V65 is in the hydrophobic pocket formed by V16, M18, V29, V44, L46, W58, L61 and V122. Two of these amino acid residues, I29V and A44V, were introduced during PSmOrange2 mutagenesis and were located in the proximity to the V65 side chain. A44V substitution led to a hydrophobic interaction of the V44 side chain with the V65 side chain. In addition, the I161V mutation was close to the phenolic ring of the chromophore. Although the I161V substitution caused the disappearance

Property	PSmOrange[a]		PSmOrange2[b]		PSmOrange3	
	Orange	Far-red	Orange	Far-red	Orange	Far-red
Absorption maximum (nm)	ND	ND	546	619	548	613
Excitation maximum (nm)	548	634	ND	ND	550	614
Emission maximum (nm)	565	662	561	651	564	655
Quantum yield[c]	0.51	0.28	0.61	0.22 ± 0.01*	0.67 ± 0.01	0.21 ± 0.01
ε ($mM^{-1}cm^{-1}$)[d]	113.3	32.7	51	22.1 ± 3.4*	55.8 ± 3.7	32.7 ± 5.2
Brightness vs. PSmOrange2 (%)[e]	186	188	100	100	120	141
pKa	6.2 ± 0.1	5.6 ± 0.1	6.6 ± 0.1	5.4 ± 0.1	6.8 ± 0.1	5.9 ± 0.1
Maturation half-time at 37°C (h)[f]	1.6		3.5		3.1	
Photobleaching half-time (s)[g]	103 ± 10[b]	1302 ± 120[b]	236 ± 18* (86 ± 2)	1814 ± 335* (667 ± 25)	2271 ± 262	1391 ± 255

Table 1. *In vitro* properties of PSmOrange3 compared to PSmOrange2. [a]Data from[7]. [b]Data from[8] except for data marked by asterisk (*). Data marked with asterisk (*) were determined in this study. [c]Quantum yields (QYs) were determined at pH 7.40. PSmOrange2 (QY = 0.61 [8]) and smURFP (QY = 0.18 [11]) and miRFP720 (QY=0.061 [12]) were used as reference standards for orange and far-red forms, respectively. [d]The extinction coefficient (ε) for the form with an absorption maximum at 548 nm was determined by alkaline denaturation. [e]Brightness was calculated as a product of the quantum yield and extinction coefficient and normalized to the brightness of PSmOrange2. [f]EGFP had a maturation half-time at 37 °C of 14 min. [g]Halftime to bleaching up to 50%. One-photon photobleaching was performed under a metal halide lamp with drops in oil. $n = 5$ and $n = 6–8$ for photobleaching experiments of the orange and far-red forms, respectively. ND, not determined. Mean ± standard deviations are reported.

of hydrophobic interaction between the side chain of this residue and the phenolic ring of the chromophore, V161 formed hydrophobic interactions with the M163 side chain in the chromophore environment and A177 (obtained as a result of the V177A mutation). Rearrangement of hydrophobic interactions of the chromophore induced by mutations resulted in a slight shift of the chromophore and tighter binding of a water molecule, which was conservative in all PSmOrange family proteins (Fig. 3 d). The other three mutations, E32K, Y208F, and M226K, were outside a β-barrel and might affect folding and maturation of PSmOrange3 (K226 is not localized in the electron density map). Thus, PSmOrange3 has a different chromophore environment with five mutations that are inner to the β-barrel. The majority of them are close to the chromophore and can define higher brightness and photostability of the orange form of PSmOrange3.

Chemical structure of PSmOrange3 chromophore probed by mass spectrometry

To elucidate the chemical structure of chromophore before and after photoconversion, we subjected the PSmOrange3 polypeptides before and after photoconversion to trypsin digestion followed by mass spectrometry analysis. The mass spectrum of PSmOrange3 trypsin-digested fragments before photoconversion revealed a triple charged m/z of 889.16 that corresponded to the monoisotopic mass of 2664.47 Da attributed to the chromopeptide. This mass was obtained after cyclization (loss of H2O) and two oxidation steps (loss of 4 H) inside the LKVTKGGPLPFAWDILSPLVTYGSK peptide. These data in combination with tandem (MS/MS) mass spectrometry confirmed the chemical structure of the mOrange-like chromophore observed earlier for mOrange[14] and PSmOrange[7] (Fig. 4a).

After photoconversion we revealed in mass spectrum the double charged m/z of 1102.05 that corresponded to monoisotopic mass of 2203.14 Da related to the chromopeptide. This mass could be obtained from the TYGSKAYVKHPADIPDYFK fragment after cleavage between the dihydrooxazole ring and CH group of valine of the GGPLPFAWDILSPLVTYGSKAYVKHPADIPDYFK fragment. MS/MS fragmentation of the TYGSKAYVKHPADIPDYFK fragment confirmed the chemical structure of the far-red chromophore that contained three rings and additional carbonyl group instead of the hydroxyl group in the dihydrooxazole ring (Fig. 4b). The same structure of the far-red chromophore was observed earlier for PSmOrange[7]. Based on mass spectrometry data, we proposed the mechanism of transformation of the orange chromophore to the far-red chromophore in PSmOrange3 (Fig. 4c).

Photoconversion of PSmOrange3 in cytosol of cultured mammalian cells

To compare the photoconversion efficiency of the PSmOrange2 and PSmOrange3 FPs, we co-expressed them with the EGFP protein via the self-cleavable P2A peptide linker in the cytosol of live HeLa cells and visualized cells under a confocal microscope (Fig. 5). Since the PSmOrange3 construct did not contain the attached nucleic export signal (NES) and PSmOrange3 has a low molecular weight of 31 kDa, PSmOrange3 was evenly distributed in the cytosol and nucleus of the HeLa cells, similarly to many others GFP-like FPs (Fig. 5a). Blue light (470/30 nm) in the range of 3 to 46 mW/mm^2 was sufficient for photoconversion of both PSmOrange2 and PSmOrange3 into a far-red state (Fig. 5b-g). The photoconversion contrast in the far-red channel was similar for both proteins (8.8 and 6 for 3 mW/mm^2; 24 and 25 for 46 mW/mm^2 for PSmOrange3 and PSmOrange2, respectively; Fig. 5c, f). However, we observed a larger decrease in the orange fluorescence after photoconversion for PSmOrange2 (Fig. 5b, e). According to the ratio of the orange fluorescence to the green fluorescence of EGFP, the orange form

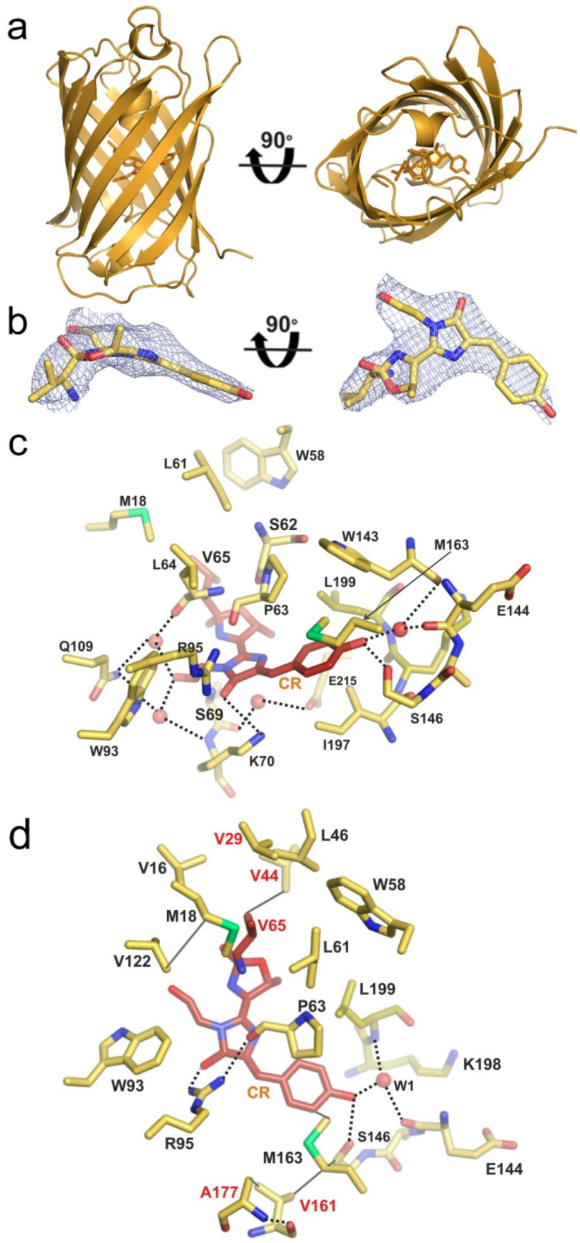

Fig. 3. X-ray structure of the PSmOrange3 protein. (**a**) Cartoon representation of the overall PSmOrange3 structure. Chromophore is shown as sticks. The orientation of the panel on the right is rotated 90° around the horizontal axis with respect to that on the left. (**b**) 2Fobs-Fcalc electron density map is shown for the chromophore of the PSmOrange3. The electron density map is shown as grey mesh and contoured at 1.1σ level. The orientation of the chromophore on the right is rotated 90° around the horizontal axis with respect to that on the left. (**c**, **d**) The immediate environment of the PSmOrange3 chromophore. (c) Possible hydrogen bond network around the PSmOrange3 chromophore is shown in black dashed lines. (**d**) Mutations in the chromophore surrounding introduced into PSmOrange2 during molecular evolution are indicated by red labels. Possible hydrophobic interactions are shown in dark-gray lines. H-bonds are shown in black dashed lines. Conservative water molecule for all proteins of PSmOrange family is shown as a red sphere and labeled as "W1".

of PSmOrange3 was 1.1–1.2 fold brighter than that of PSmOrange2 (Fig. 5 d, g). At the same time, the ratio of far-red fluorescence to green fluorescence of EGFP was the same for PSmOrange3 and PSmOrange2 (Figure S4), and hence the brightness of the far-red forms of both proteins when expressed in the cytosol was similar. Also, we checked the dependence of the far-red state brightness and ΔF/F far-red fluorescence responses depending on the wavelength of photoconversion (Fig. 5 h). ΔF/F in the far-red channel after photoconversion was 1.5- and 14-fold larger with 470/30 nm light (32 ± 1; mean ± standard deviation here and throughout) than with 433/25 nm light (21 ± 3) and 545/30 nm light (2.3 ± 1.2), respectively. Brightness of the far-red form was 1.5- and 4-fold

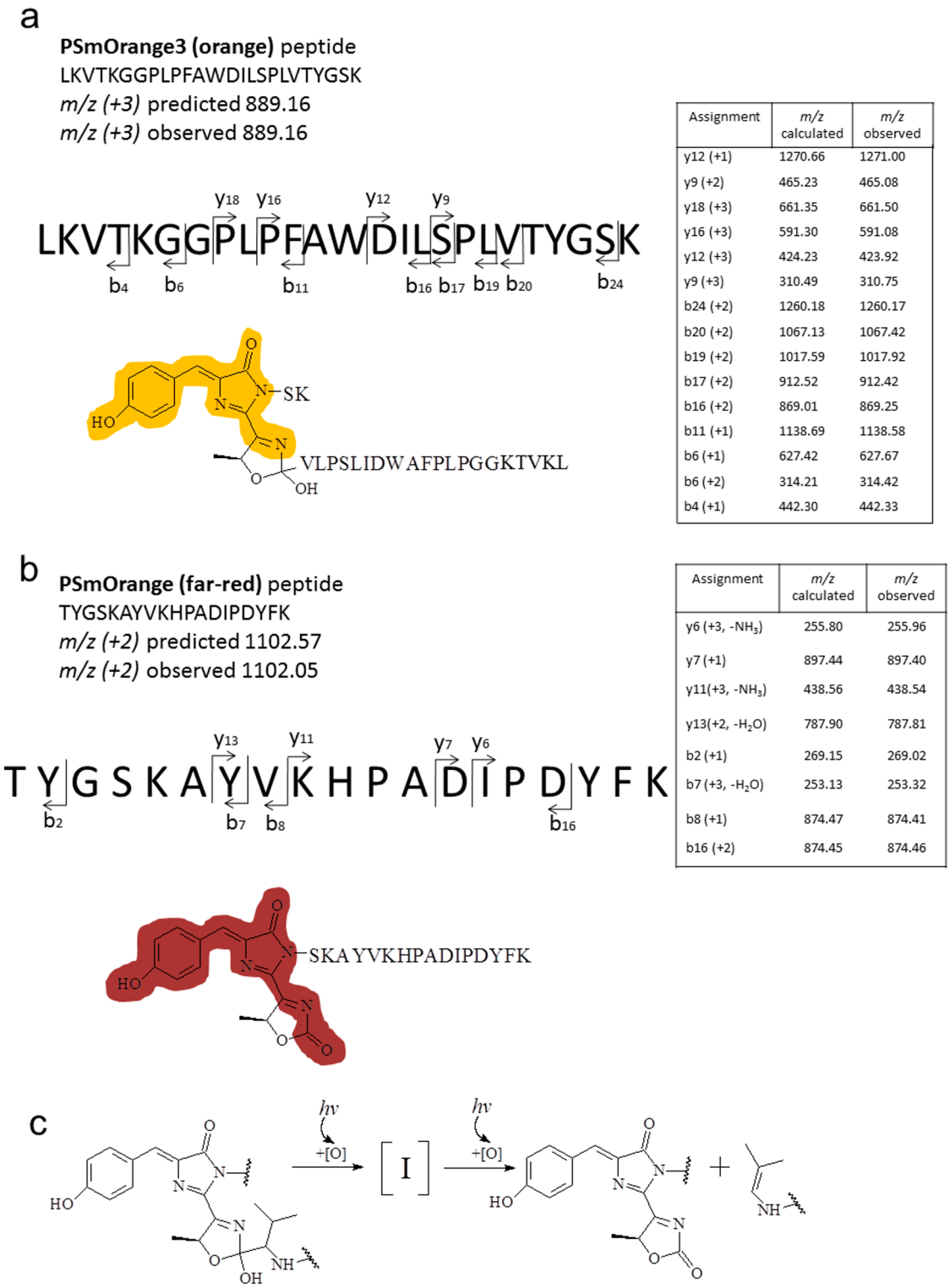

Assignment	*m/z* calculated	*m/z* observed
y12 (+1)	1270.66	1271.00
y9 (+2)	465.23	465.08
y18 (+3)	661.35	661.50
y16 (+3)	591.30	591.08
y12 (+3)	424.23	423.92
y9 (+3)	310.49	310.75
b24 (+2)	1260.18	1260.17
b20 (+2)	1067.13	1067.42
b19 (+2)	1017.59	1017.92
b17 (+2)	912.52	912.42
b16 (+2)	869.01	869.25
b11 (+1)	1138.69	1138.58
b6 (+1)	627.42	627.67
b6 (+2)	314.21	314.42
b4 (+1)	442.30	442.33

Assignment	*m/z* calculated	*m/z* observed
y6 (+3, -NH_3)	255.80	255.96
y7 (+1)	897.44	897.40
y11(+3, -NH_3)	438.56	438.54
y13(+2, -H_2O)	787.90	787.81
b2 (+1)	269.15	269.02
b7 (+3, -H_2O)	253.13	253.32
b8 (+1)	874.47	874.41
b16 (+2)	874.45	874.46

Fig. 4. Mass spectrometry analysis of the PSmOrange3 chromophore structure. (**a**, **b**) The chromophore-bearing peptides and structures of the PSmOrange3 chromophore before (**a**) and after (**b**) photoconversion. Calculated and observed m/z ratios for the orange form (**a**) and far-red form (**b**) peptides are presented in Tables. (**c**) Proposed scheme for PSmOrange3 photoconversion. [O], oxidant molecule, and *hv*, irradiation with blue (455–490 nm) light.

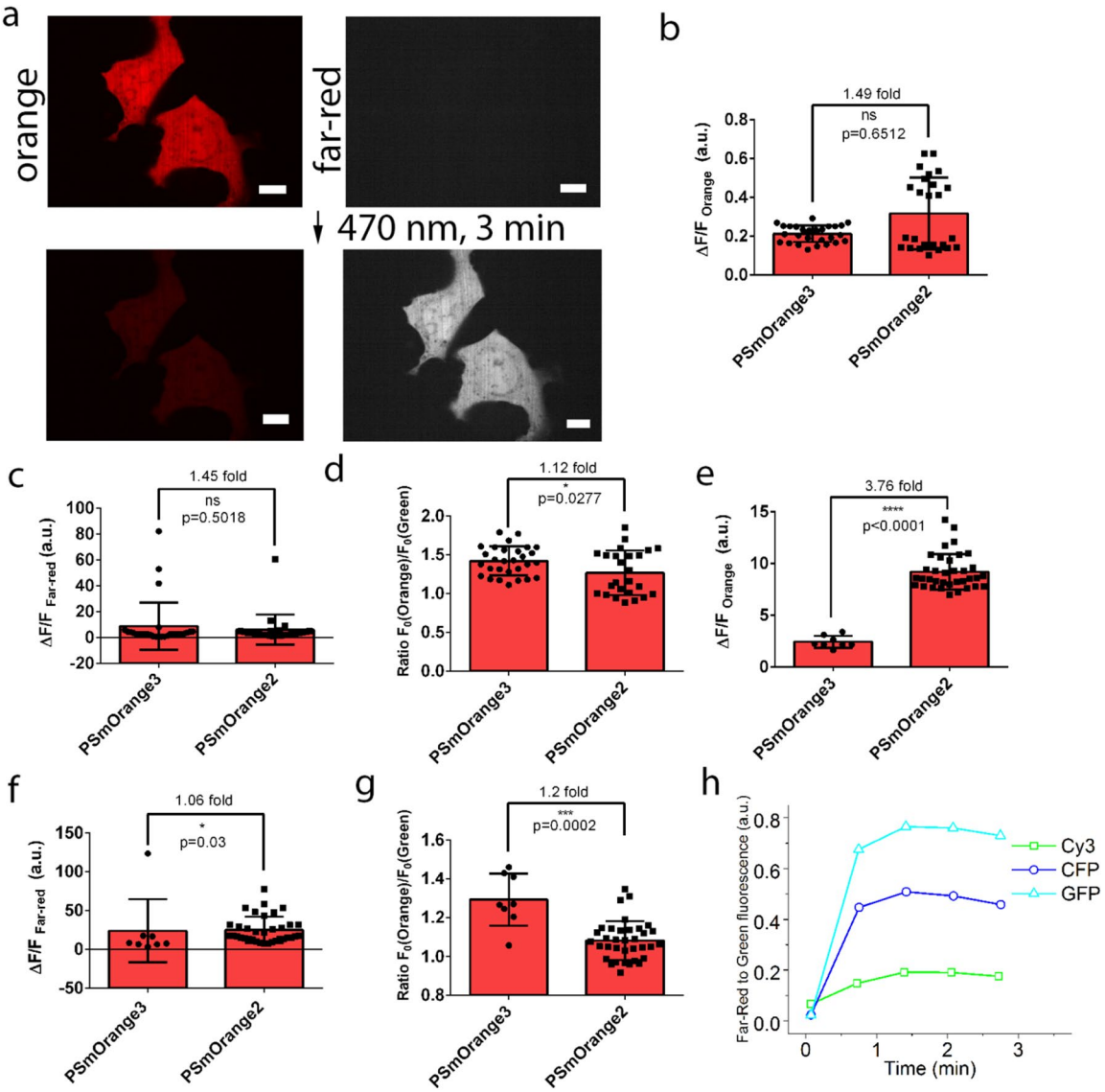

Fig. 5. Photoconversion of the PSmOrange3 protein in cytosol of HeLa cells. (**a**) Confocal images of HeLa cells expressing the PSmOrange3-P2A-EGFP protein. Red (ex: 561; em: 617/73) and far-red (ex: 640; em: 695/40) fluorescence channels are shown. Photoconversion was made with a metal halide lamp with 470/30 excitation filter, 60x, 1.4 NA oil-immersion objective, and power density in the focus of the objective 3 (**b-d**) or 46 (a, e-f) mW/mm^2. Scale bar, 10 µm. ΔF/F for orange (**b, e**) and far-red (**c, f**) forms of PSmOrange3 and PSmOrange2 upon photoconversion by 470/30 nm light. Ratio of an orange fluorescence to a green fluorescence (**d, g**). (**h**) Dependence of the far-red to green fluorescence ratio on the wavelength of the photoconversion light (GFP, CFP and Cy3 are 470/30, 433/25 and 545/30 nm excitation filters, a metal halide lamp, 60x, 1.4 NA oil-immersion objective, and power densities in the focus of the objective 46, 61 and 63 mW/mm^2 respectively.

higher after photoconversion with 470/30 nm light compared to photoconversion with 433/25 nm and 545/30 nm light, respectively. Therefore, the optimal light for photoconversion of PSmOrange3 was 470/30 nm. Both PSmOrange3 and PSmOrange2 photoconverted to the far-red state with a similar fluorescent contrast, but the orange state fluorescence dropped to a lesser extent for PSmOrange3 upon photoconversion (1.5- to 3.8-fold).

Photoconversion of PSmOrange3 in mammalian cells in fusions with structural proteins

To check the oligomeric state of PSmOrange3 in mammalian cells, we performed an organized smooth endoplasmic reticulum (OSER) assay for PSmOrange3 and compared it with the previously characterized mScarlet red fluorescent protein[13]. About 94% and 83% of HeLa cells expressing CytERM-PSmOrange3 and CytERM-mScarlet in smooth endoplasmic reticulum showed good localization of the endoplasmic reticulum net. Hence, using the OSER approach, PSmOrange3 proved to be monomeric in mammalian cells (Table S2 and Figure S5). Since the engineered PSmOrange3 showed monomeric behavior, we tested it in mammalian cells in fusions with different cytoskeletal proteins (Fig. 6 and Figure S6). To demonstrate the applicability

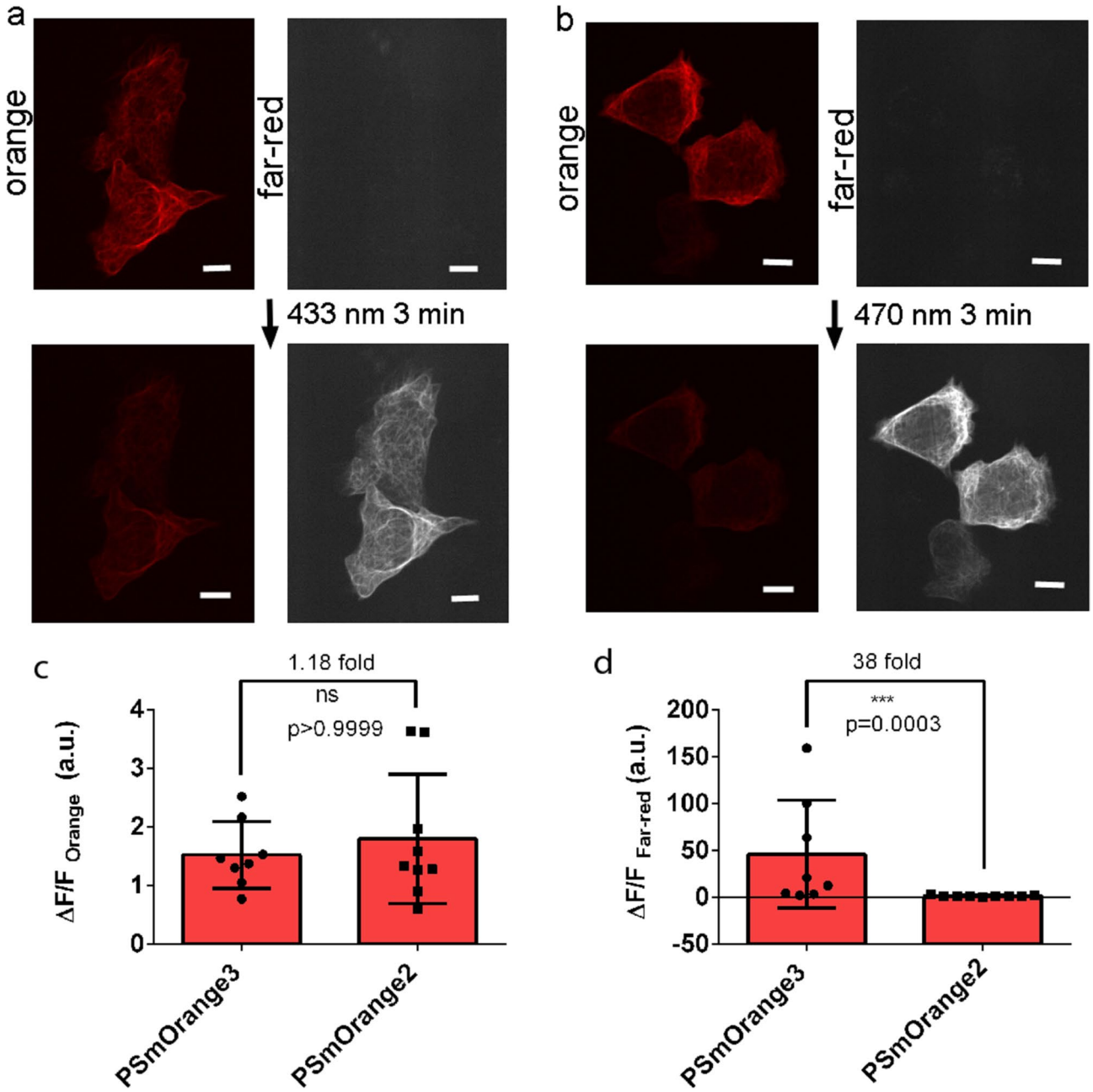

Fig. 6. Photoconversion of PSmOrange3 in fusion with EMTB. Confocal images of HeLa cells expressing the EMTB-PSmOrange3 fusion protein. Red fluorescence channel (561ex and 617/73em) for the orange form and far-red fluorescence channel (640ex and 685/40em) are shown. Photoconversion was made with a metal halide lamp with 433/25 nm (**a**) or 470/30 nm (**b**) excitation filters, 60x, 1.4 NA oil-immersion objective, and power densities in the focus of the objective 61 and 46 mW/mm^2, respectively. (**a**) ΔF/F for far-red and orange channels are 15 ± 7 and 1.2 ± 0.7 (n = 5 cells). Mean ± standard deviations are reported. (**b**) ΔF/F for far-red and orange channels are 30 ± 12 and 1.6 ± 0.7 (n = 5 cells). Mean ± standard deviations are reported. Scale bar, 10 µm. ΔF/F for orange (**c**) and far-red (**d**) forms of PSmOrange3 and PSmOrange2 upon photoconversion by 470/30 nm light.

of PSmOrange3 as a photoconvertible fluorescent probe for fluorescent microscopy, we fused it with EMTB, vimentin, and keratin and expressed fusions in HeLa cells. Standard sets of red (or Cy3) and Cy5 filters allowed the visualization of both PSmOrange3 forms without any crosstalk between the channels in fixed and live cells (Fig. 6a, b, and Fig. 7a, b). All fusions demonstrated correct localization to microtubules, intermediate filaments, and fiber-like structures (Figs. 6 and 7, and Figure S6). PSmOrange3 was successfully photoconverted into the far-red state in all fusions tested (Figs. 6 and 7, and Figure S6).

Next, we characterized photoconversion of PSmOrange3 in fusion with EMTB in more detail. To find optimal photoconversion conditions, we recorded photoconversion curves under different illumination wavelengths and

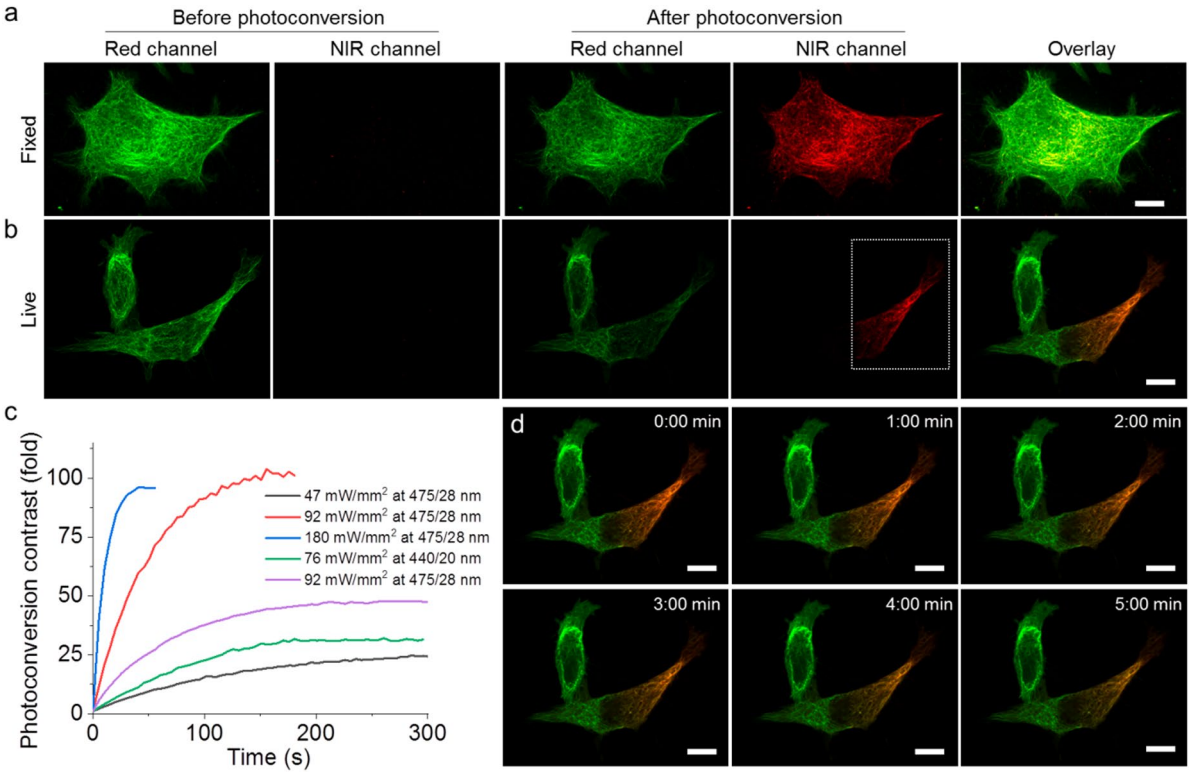

Fig. 7. PSmOrange3 can be used as a photoconvertible fluorescent probe in mammalian cells. (**a**) Representative confocal images of fixed HeLa cell expressing EMTB-PSmOrange3 fusion before and after photoconversion with 488 nm laser ($n = 15$ cells from two independent transfections). Scale bar, 10 µm. (**b**) Representative confocal images of live HeLa cells expressing EMTB-PSmOrange3 fusion before and after photoconversion with 488 nm laser under spinning disk confocal microscope ($n = 10$ cells from two independent transfections; white box indicates photoconversion area). Scale bar, 10 µm. (**c**) Photoconversion curves for PSmOrange3 expressed in fusion with EMTB in live (black, red, blue, green lines) and fixed (purple line) cells under wide-field illumination ($n = 8, 9, 5, 8, 18$ cells for 47 mW/mm^2 of 475/28 nm, 92 mW/mm^2 of 475/28 nm, 180 mW/mm^2 of 475/28 nm, 76 mW/mm^2 of 440/20 nm, 92 mW/mm^2 of 475/28 nm, respectively from 2 independent transfections each). (**d**) A time series of fluorescent images captured with 1-minute intervals showing the dynamics of the EMTB-PSmOrange3 fusion in HeLa cells ($n = 5$ cells from 2 independent transfections; photoconversion area was the same as in panel b). Scale bar, 10 µm.

intensities. First, we compared photoconversion of PSmOrange3 in its fusion with EMTB protein by violet at 433/25 nm and blue light at 470/30 nm (Fig. 6a-b). ΔF/F in the far-red channel after photoconversion was 2-fold higher with 470/30 nm light (30 ± 13) than with 433/25 nm light (15 ± 7) photoconversion. Second, we checked photoconversion of PSmOrange3 in its fusion with EMTB under different conditions. We revealed that photoconversion at 475/28 nm was about 3-fold more efficient than at 440/20 nm under comparable light intensities (Fig. 7c). Furthermore, higher 475/28 nm intensities enabled faster photoconversion with high contrasts reaching about 100-fold in 40 s under 180 mW/mm^2 (the highest power density we could achieve under the used imaging setup). We got twice as high photoconversion contrast in live cells as in fixed cells (Fig. 7c). Therefore, blue light at 470/30–475/20 nm is optimal for PSmOrange3 photoconversion.

We also compared photoconversion of PSmOrange3 and PSmOrange2 in fusion with EMTB using 470/30 nm light (Fig. 6c-d). ΔF/F fluorescence response for PSmOrange3 photoconversion was 38-fold higher (46-fold for PSmOrange3 versus 1.2-fold for PSmOrange2; Fig. 6 d). We may explain such a huge difference in this case by the high pre-photoconversion of PSmOrange2 during searching for cells in the Cy3 fluorescence channel (530–560 nm) (Figure S7). It is likely that PSmOrange2 is photoconverted more easily than PSmOrange3 by 530–560 nm light. In addition, the orange fluorescence of PSmOrange3 was brighter and required less power for searching the fluorescent cells. Hence, in the case of PSmOrange3, unlike PSmOrange2, we could hunt for the fluorescent cells in the Cy3 channel without pre-photoconversion.

We also examined the possibility of time-lapse imaging with EMTB-PSmOrange3 fusion in live mammalian cells. Photostability and brightness of both orange and far-red forms of PSmOrange3 were sufficient to perform time-lapse imaging of intracellular dynamics of the tagged protein in cells (Fig. 7 d and Supplementary Movie 1).

Evaluation of PSmOrange3 for mitochondria tracking in live HeLa cells

To benchmark the performance of PSmOrange3 against its predecessors, we compared photoconversion of PSmOrange, PSmOrange2, and PSmOrange3 in the reducing conditions of the mitochondrial lumen in two

independent series of experiments. In the first set of experiments, we estimated fluorescence responses for the far-red and orange forms of these proteins targeted to the mitochondrial inner membrane using the double mitochondrial localization signal dMito representing the N-terminal part of the cytochrome c oxidase 8 A subunit, or COX8A for short, in HeLa cells (Figure S8). All three dMito-PSmOranges fusion proteins were properly localized to mitochondria. Under identical photoconversion conditions, PSmOrange3 had the highest ΔF/F fluorescence response for the far-red state (9.7 ± 7.4) that was 5.5- and 2.1-fold higher than those for PSmOrange2 (1.8 ± 0.7) and PSmOrange (4.6 ± 3.6), respectively (Figure S8b). The ΔF/F fluorescence responses for the orange forms were similar in the case of PSmOrange3 (1.3 ± 0.7) and PSmOrange (1.5 ± 0.8), but they were about 2-fold higher than for PSmOrange2 (0.7 ± 0.2) (Figure S8c). Compared to the cytoplasm of HeLa cells, the reducing environment of the mitochondrial lumen most severely reduced the photoconversion efficiency for the PSmOrange2 and less affected the photoconversion efficiencies for PSmOrange and PSmOrange3.

In the second series of experiments, we compared photoconversion kinetics for three PSmOrange proteins targeted to the mitochondrial inner membrane using the COX8A tag in HeLa cells, depending on the illumination wavelength (Fig. 8). PSmOrange3 outperformed PSmOrange and PSmOrange2 in the brightness of orange form before photoconversion, as well as far-red form after photoconversion (Fig. 8a, b). Upon photoconversion with 475/28 nm light, PSmOrange and PSmOrange3 exhibited similar photoconversion contrast of ~ 240-fold for their far-red forms, with PSmOrange photoconversion being twice faster (photoconversion half-time of 80 s for PSmOrange vs. 160 s for PSmOrange3; Fig. 8c, Supplementary Movie 2). PSmOrange2 in the reducing conditions had about 3-fold lower photoconversion contrast (83-fold) compared to PSmOrange3, with photoconversion kinetics matching that of PSmOrange (photoconversion half-time of 71 s). When 555/28 nm light, used also for imaging of the orange forms, was applied for photoconversion, PSmOrange photoconverted efficiently with ~ 10-fold contrast, which was 4.3- and 6.6-fold higher than for PSmOrange2 and PSmOrange3, respectively (Fig. 8 d). Thus, in the reducing conditions of the mitochondrial lumen, PSmOrange3 was the brightest in the PSmOrange series, and had the highest and the lowest ΔF/F fluorescence responses upon blue and green light photoconversion, respectively. The last property allows to follow the orange form of PSmOrange3 in one fluorescent channel and photoconvert it to the far-red form under blue light, followed by dual-color live cell imaging of both orange and far-red forms to track mitochondria dynamics for at least 20 min (Supplementary Movie 3). Moreover, imaging and photoconversion of PSmOrange3 can be combined with bright and photostable green FPs, such as mBaoJin[15]. In this case, mBaoJin can be imaged at low excitation power densities (~ 1–2 mW/mm^2) without considerable PSmOrange3 photoconversion, while higher power illumination required for photoconversion did not photobleach mBaoJin (Fig. 8e), enabling three-color live cell imaging without interference between channels (Supplementary Movie 4).

Evaluation of PSmOrange3 as a probe for photoactivated localization microscopy

Next, we evaluated the single-molecule characteristics of PSmOrange3. We fused PSmOrange3 to EMTB, expressed the constructs in HeLa cells, and imaged the PFA-fixed and live cells using photoactivated localization microscopy (PALM) under high 642 nm excitation (6.9 kW/cm^2). A 488 nm laser was used for photoconversion, and the intensity was manually increased to maintain sparsely blinking molecules. The single-molecule statistics indicated that the photostability of the far-red form of PSmOrange3, the photon statistics and localization precision of the photoconverted PSmOrange3 molecules had properties sufficient for PALM imaging (Fig. 9).

Next, we conducted a side-by-side comparison of the PSmOrange3 performance with its predecessors, the PSmOrange and PSmOrange2 proteins, under PALM microscopy. EMTB-PSmOrange, EMTB-PSmOrange2, and EMTB-PSmOrange3 fusions were transiently transfected in HeLa cells and imaged in 48 h using 488 nm photoconversion and 640 nm excitation lights. Photostability, signal-to-noise ratio, localization precision, and photon counts were similar between the three tested proteins (Fig. 10). Hence, all three fluorescent proteins demonstrated similar single-molecule properties in PALM microscopy.

Conclusions

In conclusion, we engineered and characterized in vitro and in mammalian cells photoconvertible orange-to-far-red fluorescent protein PSmOrange3. Both orange and far-red forms are 1.2–1.4-fold brighter than those forms of the original PSmOrange2 (**Table 1**). In addition, an orange form of PSmOrange3 is 10-fold more photostable, but a far-red form is 1.3-fold less photostable than for PSmOrange2. pH stabilities and maturation rates for PSmOrange2 and PSmOrange3 are similar. As PSmOrange3 was developed without application of external oxidants, it had the highest ΔF/F fluorescence response for its far-red form and brightness of both forms among all three proteins of PSmOrange series in the reducing environment of mitochondria. In addition, PSmOrange3 was efficiently photoconverted with blue (455–490 nm) light and almost was not photoconverted with green (535–565 nm) light used for imaging of the orange form. This property gives an opportunity to perform imaging of the orange form and photoconversion to the far-red state using different light. All three proteins PSmOrange, PSmOrange2 and PSmOrange3 showed similar properties to each other at the single-molecule level under PALM microscopy.

Materials and methods

Cloning of bacterial vectors, mutagenesis and library screening

PSmOrange proteins were cloned into the pBAD/HisB plasmid (Invitrogen) at BglII/EcoRI restriction sites using the Fw-LSSmOrange-BglII/Rv-LSSmOrange-EcoRI primers listed in Table S3 to express PSmOranges proteins in BW25113 bacterial cells (kindly provided by Verkhusha V.V. from Albert Einstein College of Medicine, NY, USA).

Random libraries of PSmOrange2 were generated and expressed as described earlier[15].

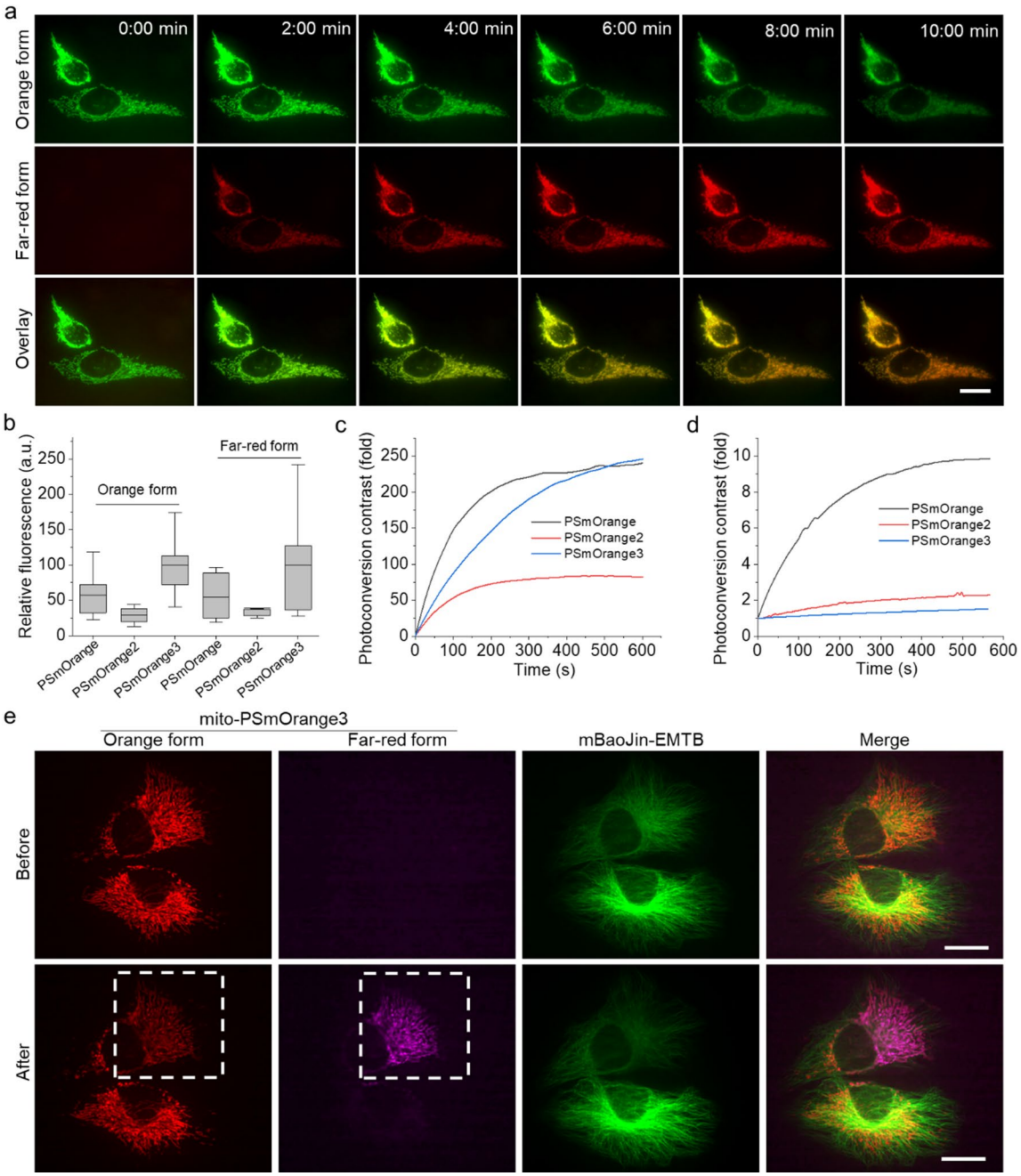

Fig. 8. Photoconversion properties of PSmOrange3 in mitochondria of live HeLa cells under wide-field illumination compared to PSmOrange and PSmOrange2. (**a**) Representative time-lapse images of orange and far-red forms of PSmOrange3 during photoconversion under 475/28 nm light. Scale bar, 20 μm. (**b**) Quantification of fluorescence intensity of orange and far-red forms of PSmOrange, PSmOrange2, and PSmOrange3 before and after photoconversion, respectively, under identical conditions. (**c**) Photoconversion kinetics under 475/28 nm light at ~ 50 mW/mm^2. (**d**) Photoconversion kinetics under 555/20 nm light at ~ 10 mW/mm^2. (**e**) Representative HeLa cells coexpressing the COX8A-PSmOrange3 and EMTB-mBaoJin fusions before and after spatially selective photoconversion was under 475/28 nm light. Scale bar, 20 μm.

Screening of bacterial libraries was performed on Petri dishes under a fluorescent microscope. Briefly, expression of the PSmOranges on the colonies on Petri dishes was induced with 0.02% arabinose for 24 h at 37 °C. Screening of about 10,000 colonies of the bacterial library expressing PSmOranges variants was performed on Petri dishes under a fluorescent stereomicroscope Leica M205FA (Leica, Germany) equipped with the DFC310FX camera (Leica Microsystems, Germany) and mercury metal halide light source EL6000 (Leica Microsystems, Germany). For screening on Petri dishes, bacterial colonies with the highest ratio of fluorescence in the far-red channel (excitation at 620/60 nm and emission at 700/75 nm) after illumination with LED array at 463/16 nm, 200 mW/cm^2 to a far-red fluorescence before illumination were picked for streaking on the fresh

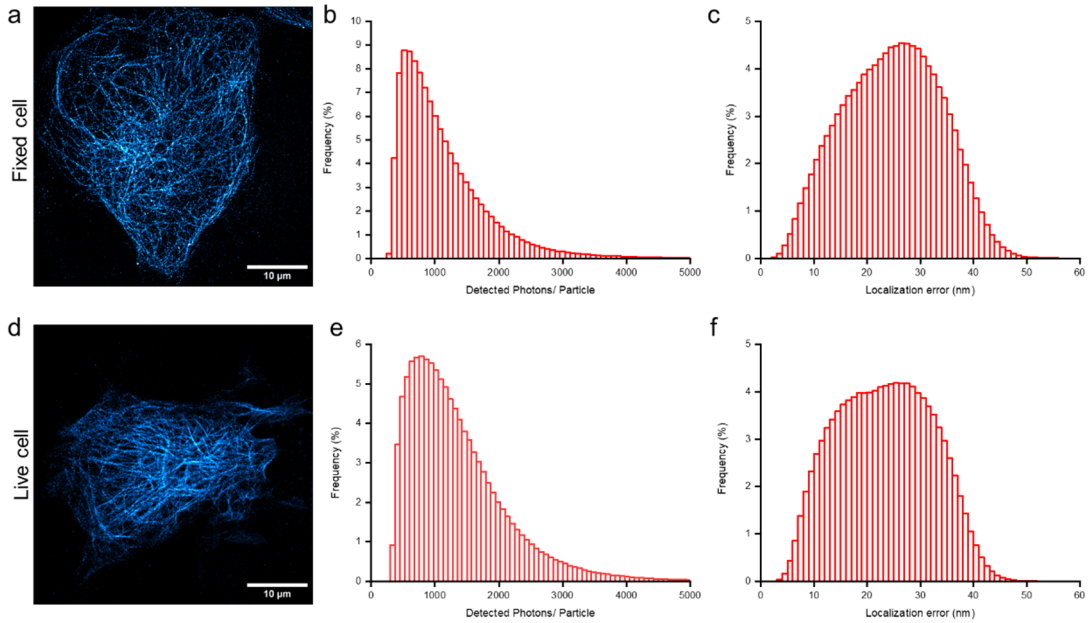

Fig. 9. PALM imaging and single-molecule analysis of PSmOrange3 Fusion with α-tubulin in fixed and live HeLa cells. (**a**) A representative PALM image reconstructed from 18,810 consecutive frames of photoconverted PSmOrange3 in fixed cells ($n = 12$ cells from one transfection). (**b**) Distribution of the total number of photons from PSmOrange3 for the image shown in a (mean 1,078, median 892). (**c**) Localization precision per single-molecule event for the image shown in a (mean 24.6 nm, median 24.7 nm). (**d**) A representative PALM image reconstructed from 10,879 consecutive frames of photoconverted PSmOrange3 in live cells ($n = 8$ cells from one transfection). (**e**) Distribution of the total number of photons from PSmOrange3 for the image shown in d (mean 1,353, median 1,173). (**f**) Localization precision per single-molecule event for the image shown in d (mean 23.3 nm, median 23.4 nm).

Petri dishes. Acquired images were analyzed using ImageJ 1.45s software (https://imagej.net/ij/), and 150–200 colonies having the highest ratios were picked up for further analysis on Petri dishes with streaks. Next, streaks of the selected clones on Petri dishes were analyzed following the same protocol as used for colonies. The best 5–10 clones were selected for sequencing. For the next round, we chose 1–3 clones with different mutations.

The mammalian plasmids, including fully annotated and verified sequences, generated in this study are available from the WeKwikGene plasmid repository at Westlake Laboratory (https://wekwikgene.wllsb.edu.cn/) with following barcodes: pEMTB-PSmOrange #0000339; pAAV-dMito-PSmOrange2 #0000578; pAAV-dMito-PSmOrange #0000579; pAAV-dMito-PSmOrange3 #0000580; pCytERM-PSmOrange3 #0000683; pEMTB-PSmOrange3 #0000684; pAAV-CAG-PSmOrange3-P2A-EGFP #0000685.

Proteins' purification and characterization

Purification and characterization of PSmOrange3, and preparative purification of PSmOrange3 protein for X-ray crystallography was performed as described earlier[16].

The absorption spectra were recorded using NanoDrop 2000 spectrophotometer (Thermo Fisher Scientific, USA). Excitation and emission spectra were measured with a CM2203 spectrofluorometer (Solar, Belarus).

Chromophore extinction coefficient for the orange form of the purified PSmOrange3 was measured in the phosphate buffer saline (PBS) by alkaline denaturation with 1 M NaOH and using extinction coefficient for GFP-like chromophore equal to 44,000 M^{-1} cm^{-1} in 1 M NaOH[17]. Extinction coefficients for the far-red forms of PSmOrange3/2 were measured after photoconversion of the purified proteins in 1 mM $K_3Fe(CN)_6$ using 463/17 nm LED, 200 mW/cm^2 for 1–3 min on ice. Absorption spectra were recorded before and after photoconversion, then the extinction coefficients of the far-red forms were calculated using the extinction coefficients of the orange forms, decrease of the orange form absorption value at the maximum (548 nm) and increase of the far-red form absorption value at the maximum (613 nm) after photoconversion.

For quantum yield determination, the integrated fluorescence values of the purified PSmOrange3 before and after photoconversion were measured in PBS, and were compared with the integrated fluorescence values of the equally absorbing PSmOrange2 without photoconversion (quantum yield of 0.61)[8] or smURFP (quantum yield of 0.18)[11], respectively.

For determination of the pH dependences, the orange or the far-red forms of PSmOrange3 (5 µM) were diluted 1:100 into a series of pH adjusted buffers (30 mM citric acid, 30 mM borax, or 30 mM NaCl) with pH values ranging from 9 to 3 in 0.5 pH units interval in a 96-well black clear bottom plate (Thermo Scientific, USA). Fluorescence was measured using a ModulusTM II Microplate Reader (TurnerBiosystems, USA).

Photobleaching experiments were performed with suspensions of purified proteins in mineral oil, as previously described[18,19]. Briefly, the kinetics of photobleaching was measured using purified proteins in PBS

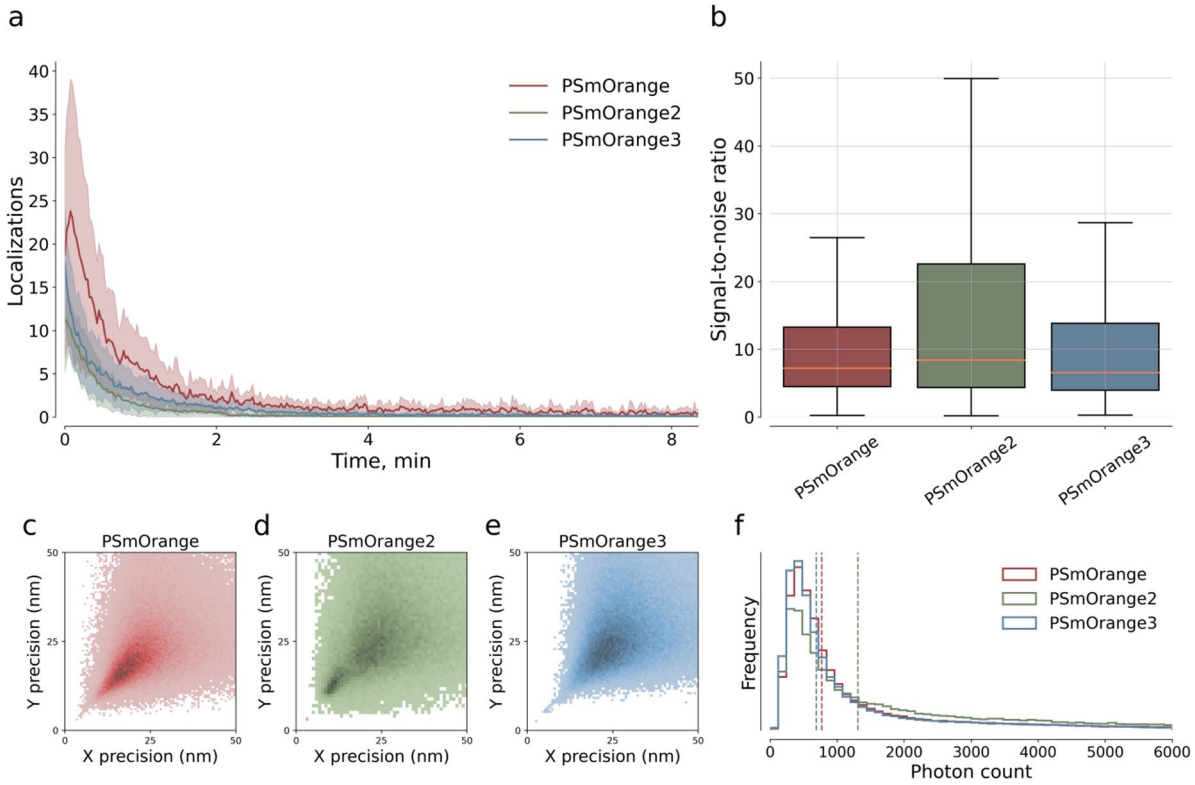

Fig. 10. Comparison of the PSmOrange, PSmOrange2, and PSmOrange3 proteins performance in PALM imaging of their fusions with ensconsin microtubule binding domain (EMTB) protein in live HeLa cells. Images were acquired with Nanoimager S microscope using 157.5 W/cm^2 488 nm laser for phoconversion and 6.3 kW/cm^2 640 nm laser for acquisition, 10,000 frames with 50 ms exposure time. $N = 5–10$ regions of interest from 5–10 cells (from 1 independent culture) per fluorescent protein. (**a**) Stability of localization density for PSmOrange, PSmOrange2 and PSmOrange3. Data shown as mean (solid line) ± SD (filled area). (**b**) Signal-to-noise ratio of localizations in selected regions of interest. The boxes are the first and the third quartiles, whiskers are the rest of the distribution except outliers, the orange line is the median. (**c**-**e**) 2D histograms of localization precision per single-molecule event. (**f**) Histogram of frequency distribution of localizations with various intensity. Vertical dotted lines represent median values.

at 45 μM concentration, in aqueous microdroplets in mineral oil using Zeiss Axio Imager Z2 microscope (Zeiss, Germany) equipped with a 120 W mercury short-arc lamp (OSRAM, Czech Republic), a 63 × 1.4 NA oil immersion objective lens (PlanApo, Zeiss, Germany), a 550/25BP excitation, and a 605/70BP emission filters for the orange form; and a laser spinning-disk Andor XDi Technology Revolution multi-point confocal system (Andor, UK) equipped with an inverted Nikon Eclipse Ti microscope, a 120 W mercury short-arc lamp (OSRAM, Czech Republic), 60 × 1.4 NA oil immersion objective lens (PlanApo, Zeiss, Germany), a 620/60BP excitation, and a 685/40BP emission filters for the far-red form. Light power density measured at the focus of the objective lens was 53 and 0.56 mW/mm^2 for the orange and the far-red forms, respectively. The times to photobleach from 100 down to 50 percents were calculated[19].

To obtain the photoconversion quantum yield Φ, we used the Eq. (1)[20]:

$$k_{\text{fit}}\, c_0 \;=? * I_0\,(1 - 10^{-A\prime\, i}) \tag{1}$$

where k_{fit}, c_0, I_0 and A'_i are the time constant, the concentration of the protein, light intensity and the initial absorption of the protein at the irradiation wavelength.

We regarded LED as monochromatic light source and used the Eq. (2)[20] to translate the radiant power into a photon flux I_0 in mol L^{-1} s^{-1}:

$$I_0 \;= \lambda * P_{\text{LED}} / \,(h^* c^* N_{\text{A}}^* V) \tag{2}$$

Here, λ is the peak wavelength of the LED (in m), h is Planck's constant (h = 6.63 × 10^{-34} J s), c is the speed of light in a vacuum (c = 299 792 458 m s^{-1}), N_A is Avogadro's constant (N_A = 6.02 × 10^{23} mol^{-1}) and V is the reaction volume (in L).

We carried out photoconversion of PSmOrange2 and PSmOrange3 with LED at 463/17 nm. k_{fit} for the orange or the far-red forms were determined as the slopes of the initial linear sections of the time dependences of the orange or the far-red fluorescence, respectively. The time constants k_{fit} were determined for several power

densities of LED. Then we built the linear dependencies of $k_{fit}\,c_0$ from $I_0\,(1–10^{-A'i})$. The photoconversion quantum yields Φ were determined as the slopes of these linear dependencies.

To study protein maturation, BW25113 bacteria transformed with the pBAD/HisB-PSmOrange3 plasmid were grown in LB medium supplemented with ampicillin at 37 °C overnight. The next morning 0.2% arabinose was added to bacterial cells. Upon induction of protein expression, bacterial cultures were grown at 37 °C in 15 ml tubes filled to the brim and tightly sealed to restrict oxygen supply. After 3 h, the cultures were centrifuged in the same tightly closed tubes. After opening the tubes, the bacteria were sonicated in 800 µl of PBS buffer supplemented with chloramphenicol to prevent additional translation of the PSmOrange3 protein and precipitated for 5 min at 15,000 rpm at 4 °C. 100 µl of the resulting protein lysate was added to 2.9 ml of PBS supplemented with chloramphenicol. Protein maturation measured at 37 °C using orange fluorescence signal with excitation and emission at 540 nm and 570 nm, respectively, with a CM2203 spectrofluorometer (Solar, Belarus).

Size-exclusion chromatography was performed with a SuperdexTM 200 10/300 GL column using GE ÄKTA Explorer (Amersham Pharmacia, UK) FPLC System. The concentration of the purified PSmOrange3 protein was 10 mg/ml.

Protein crystallization

Initial crystallization conditions for PsmOrange3 were found using Oryx4 robotic system (Douglas Instruments) and commercially available 96-well crystallization screens (Hampton Research, Aliso Viejo, CA, USA and Anatrace, Maumee, OH, USA). The PsmOrange3 crystal used for diffraction data collection was obtained after 1 month at 288 K by vapor diffusion method in 1.4 M sodium/potassium phosphate pH 8.2.

Data collection, processing, structure determination, and refinement

Before data collection crystal was transferred to a cryoprotection solution consisting of the same components as the reservoir solution and 25% glycerol and frozen in liquid nitrogen. The 2.8Å data were collected at 100 K at BL10U2 beamline (SSRF, Shanghai, China). The data were indexed and integrated using the XDS program[21] and scaled using Aimless program of CCP4 package[22] (Table S1).

The structure was solved by the molecular replacement method using fluorescent protein PSmOrange (PDB ID: 4Q7T) as an initial model by the MOLREP program[23]. The refinement of the structure was carried out using the REFMAC5 [22]. The visual inspection of electron density maps and the manual rebuilding of the model were carried out using the COOT program[24]. PsmOrange3 was obtained in space group $P3_221$. The asymmetric unit contains one molecule. The structure was deposited in the Protein Data Bank under accession code 9IRJ.

Mass spectrometry

The samples were digested with trypsin (V5280, Promega, Madison, WI, USA) in accordance with the manufacturer's protocol. Briefly, the protein was hydrolyzed with trypsin at an enzyme/protein ratio of 1:50 (2 µg of trypsin/100 µg of protein) for 16 h at 37 ∘C. The reaction was stopped by adding formic acid to a final concentration of 0.1%. HPLC-MS/MS experiments were carried out on a Dionex Ultimate 3000 XRS (Thermo Fisher Scientific, USA) coupled to hybrid Orbitrap Elite (Thermo Fisher Scientific, USA) high resolution mass spectrometer. The sample volume loaded was 2 µL per injection. HPLC separation was carried out using Phenomenex Aeris Peptide XB-C18 (150мм x 2,1мм x 1.7мкм) by gradient elution. Mobile phase A was 0.1% formic acid in water; mobile phase B was 0.1% formic acid in acetonitrile. LC separation was achieved at a flow of 250 nL/min using a 30 min gradient from 5 to 55% of phase B.

Mammalian plasmids construction

In order to construct the pAAV-*CAG*-PSmOrange1/2/3-P2A-EGFP plasmids, the PSmOranges genes were PCR amplified as the KpnI-AgeI fragments, using LSSCy-KpnI/PSO3-AgeI-r2 primers listed in the Table S3, and swapped the miRFP720 gene in the pAAV-miRFP720-P2A-EGFP vector.

In order to construct the pLU-CMV-vimentin-PSmOrange3 plasmid, the PSmOrange3 gene was PCR amplified as the BamHI-BsrGI fragment, using KpnI-PSO3/PSO3-BsrGI-r primers listed in the Table S3, and swapped the NeonOxIrr gene in the pLU-CMV-vimentin-NeonOxIrr vector[25].

In order to construct the pKeratin-PSmOrange3 plasmid, the PSmOrange3 gene was PCR synthetized as the KpnI-NotI fragment, using KpnI-PSO3/NotI-PSO3-r primers listed in the Table S3, and inserted in the pKeratin-mKate2 vector[26] at KpnI/NotI restriction sites.

In order to construct the pEMTB-PSmOrange1/2/3 plasmid, the PSmOrange1/2/3 genes were PCR synthetized as the AgeI-NotI fragment, using AgeI-PSO3/NotI-PSO3-r primers listed in the Table S3, and inserted in the pEMTB-mNeonGreen vector described above at AgeI/NotI restriction sites.

In order to construct the pdMito-PSmOrange1/2/3 plasmids, the PSmOrange 1/2/3 genes were PCR amplified as the XhoI-EcoRI fragments, using LSSmSc-XhoI/Rv-LSSmOrange-EcoRI primers listed in the Table S3, and inserted in the pdMito-mCherry vector at XhoI/EcoRI restriction sites.

Cell culture

HeLa Kyoto cells, used in Figs. 4, 5, 7b and 9, and Figure S2, S3, S4, were kindly provided by Vsevolod V. Belousov (Shemyakin-Ovchinnikov Institute of Bioorganic Chemistry, Russian Academy of Sciences, Moscow, 117997, Russia). HeLa cells, used in Figs. 7, 8a, c, d and e and 9, and Supplementary Movies 1,2,3,4, were obtained from American Type Culture Collection (ATCC CCL-2). HeLa cells were authenticated by the manufacturer using short tandem repeat profiling, reauthenticated in the Subach laboratory (HeLa Kyoto cells) and in the Piatkevich laboratory (HeLa ATCC CCL-2) by inspecting stereotypical morphological features under a widefield microscope, and tested negative for Mycoplasma contamination to standard levels of stringency. Authentication

by morphology was performed every time before transient transfection. HeLa cells were grown in DMEM (Gibco, catalog no. C11965500CP), supplemented with 10% fetal bovine serum (Sigma-Aldrich, catalog no. F8318-500ML) and 1% penicillin-streptomycin (Gibco, catalog no. 15140-122) at 37 °C with 5% CO_2.

Transfection

HeLa cells expressing pPSmOrange1/2/3-P2A-EGFP, pEMTB-PSmOrange1/2/3, vimentin-PSmOrange3, keratin-PSmOrange3, dMito-PSmOrange1/2/3 and COX8A-PSmOrange1/2/3 were transiently transfected with FuGene HD transfection reagent (FuGENE, catalog no. HD-1000) or as described earlier[16]. Transfection for PALM imaging was performed as suggested by the manufacturer with a modification of 5 µl of transfection reagent and 1 µg of DNA per well in a six-well plate. The day before transfection, cells were plated on poly-l-lysine coated (Sigma-Aldrich, catalog no. P4707) coverslips (Marienfeld, catalog no. 0117650).

Live cell preparation

The culture medium was removed and the sample was washed with 1× PBS three times. Afterward, 1 ml of live cell imaging solution (Gibco, catalog no. A18967-01) was added to the sample, with the additional glucose to achieve a final concentration of 15 mM. Finally, the sample was transferred for live cell imaging.

Cell fixation

Cells were fixed with 3% formaldehyde (PFA; Electron Microscopy Sciences, catalog no. 15710) and 0.1% glutaraldehyde (GA; Electron Microscopy Sciences, catalog no. 16020) in 1× PBS for 15 min at RT. Samples were rinsed three times with 1× PBS before stored in 1× PBS at 4 °C.

Imaging of mammalian cells

HeLa Kyoto cell cultures were imaged 48 h after transfection using a laser spinning-disk Andor XDi Technology Revolution multi-point confocal system (Andor, UK) equipped with an inverted Nikon Eclipse Ti microscope, a 120 W mercury short-arc lamp (OSRAM, Czech Republic), a 60× oil immersion objective (Nikon, Japan), a 16-bit QuantEM 512SC electron-multiplying CCD (Photometrics, USA), and a cage incubator (Okolab, Italy). 470/30, 433/25 and 545/30 nm excitation filers, a metal halide lamp, 60x, 1.4 NA oil-immersion objective, and power in the focus of the objective 46, 61 and 63 mW/mm^2 were used for photoconversion of PSmOrange2/3. Red fluorescence channel (561ex and 617/73em) and far-red fluorescence channel (640ex and 685/40em) were used for imaging of the orange and far-red forms, respectively. A power density of light was estimated in a focal plane of a 60 × 1.4 NA oil immersion objective lens (UPlanSApo, Olympus). For each region of interest we calculated ΔF/F fluorescence response for the selected area of each cell, where $\Delta F/F = F_{max}/F_0 - 1$, F_{max} and F_0 are maximal (saturated value after photoconversion for the far-red form and initial value for the orange form) and minimal (saturated value after photoconversion for the orange form and initial value for the far-red form) fluorescence values.

PALM imaging

Photoactivated Localization Microscopy (PALM) imaging was conducted using a custom-built microscope equipped with an oil objective (100×/1.5NA, UPLAPO100XOHR, Olympus, Japan). The excitation lasers utilized were a 642 nm 2 W laser (MPB Communications, 2RU-VFL-2000-642-B1R) and a 488 nm 150 mW laser (Coherent, OBIS 488 nm LS 150 mW). The power density at the sample plane for the 642 nm laser was approximately 6.9 kW/cm^2. The intensity of the 488 nm laser was manually increased during the acquisition process. A quadruple-band dichroic mirror (ZT405/488/561/640 rpcv2, Chroma) was employed, and the emitted light was further filtered using a band-pass filter with a center wavelength of 700 nm (ET700/75m, Chroma).

Data for Fig. 8 was acquired with Nanoimager S (ONI, UK) equipped with UPlanSApo 100 × 1.4NA oil immersion lens (Olympus), 488 nm and 640 nm lasers, 560 nm dichroic mirror and Scope8 sCMOS camera. Images were captured in TIRF regime using 488 nm laser for photoconversion (≈ 157.5 W/cm^2) and 640 nm laser for excitation (≈ 6.3 kW/cm^2). A series of multiple images (10000 frames) were obtained at 20 fps with 1 activation frame followed by 10 acquisition frames. Image acquisition was performed using NimOS 1.18.3.15066.

Image processing and data analysis were performed using NimOS 1.7.3.10248 and custom-made Python 3.9 scripts with pandas (ver. 1.2.4), numpy (ver. 1.22.4), matplotlib (ver. 3.7.2), seaborn (ver. 0.13.2), scipy (ver. 1.6.2) and opencv (ver. 4.5.5.62) packages. Image reconstruction was performed using default parameters of initial sigma.

Data availability

The PDB ID of the PSmOrange3 atomic structures is 9IRJ (https://doi.org/10.2210/pdb9irj/pdb). The total size of the files acquired for this study exceeds the 20-GB limit of the FigShare repository; therefore, only the most essential raw datasets, including source files for supplementary figures and raw unprocessed images, will be available at FigShare upon acceptance of the manuscript. The remaining files are available from the corresponding author upon request. All plasmids used in this study are available from WeKwikGene (https:/wekwikgene.wllsb.edu.cn/) with following barcodes: pEMTB-PSmOrange #0000339; pAAV-dMito-PSmOrange2 #0000578; pAAV-dMito-PSmOrange #0000579; pAAV-dMito-PSmOrange3 #0000580; pCytERM-PSmOrange3 #0000683; pEMTB-PSmOrange3 #0000684; pAAV-CAG-PSmOrange3-P2A-EGFP #0000685. Source data will be provided with this paper.

Received: 26 June 2025; Accepted: 9 October 2025
Published online: 17 November 2025

References

1. Chudakov, D. M., Lukyanov, S. & Lukyanov, K. A. Tracking intracellular protein movements using photoswitchable fluorescent proteins PS-CFP2 and Dendra2. *Nat. Protoc.* **2**, 2024–2032 (2007).
2. McKinney, S. A., Murphy, C. S., Hazelwood, K. L., Davidson, M. W. & Looger, L. L. A bright and photostable photoconvertible fluorescent protein. *Nat. Methods*. **6**, 131–133 (2009).
3. Zhang, M. et al. Rational design of true monomeric and bright photoactivatable fluorescent proteins. *Nat. Methods*. **9**, 727–729 (2012).
4. Habuchi, S., Tsutsui, H., Kochaniak, A. B., Miyawaki, A. & van Oijen, A. M. mKikGR, a monomeric photoswitchable fluorescent protein. *PLoS One*. **3**, e3944 (2008).
5. McEvoy, A. L. et al. mMaple: a photoconvertible fluorescent protein for use in multiple imaging modalities. *PloS One*. **7**, e51314 (2012).
6. Hoi, H. et al. A monomeric photoconvertible fluorescent protein for imaging of dynamic protein localization. *J. Mol. Biol.* **401**, 776–791 (2010).
7. Subach, O. M. et al. A photoswitchable orange-to-far-red fluorescent protein, psmorange. *Nat. Methods*. **8**, 771–777 (2011).
8. Subach, O. M., Entenberg, D., Condeelis, J. S. & Verkhusha, V. V. A FRET-facilitated photoswitching using an orange fluorescent protein with the fast photoconversion kinetics. *J. Am. Chem. Soc.* **134**, 14789–14799 (2012).
9. Pletnev, S. et al. Orange fluorescent proteins: structural studies of LSSmOrange, psmorange and psmorange2. *PloS One*. **9**, e99136 (2014).
10. Ruchkin, D. A. et al. Two key substitutions in the chromophore environment of mKate2 produce an enhanced FusionRed-like red fluorescent protein. *Acta Naturae*. **17**, 110–117 (2025).
11. Rodriguez, E. A. et al. A far-red fluorescent protein evolved from a cyanobacterial Phycobiliprotein. *Nat. Methods*. **13**, 763–769 (2016).
12. Shcherbakova, D. M., Cox Cammer, N., Huisman, T. M., Verkhusha, V. V. & Hodgson, L. Direct multiplex imaging and optogenetics of Rho GTPases enabled by near-infrared FRET. *Nat. Chem. Biol.* **14**, 591–600 (2018).
13. Bindels, D. S. et al. mScarlet: a bright monomeric red fluorescent protein for cellular imaging. *Nat. Methods*. **14**, 53–56 (2017).
14. Shu, X., Shaner, N. C., Yarbrough, C. A., Tsien, R. Y. & Remington, S. J. Novel chromophores and buried charges control color in mFruits. *Biochemistry* **45**, 9639–9647 (2006).
15. Zhang, H. et al. Bright and stable monomeric green fluorescent protein derived from StayGold. *Nat. Methods*. **21**, 657–665 (2024).
16. Subach, O. M. et al. Novel genetically encoded bright positive calcium indicator NCaMP7 based on the mNeonGreen fluorescent protein. *Int J. Mol. Sci* **21**, 1644-1667(2020).
17. Subach, F. V. et al. Photoactivatable mCherry for high-resolution two-color fluorescence microscopy. *Nat. Methods*. **6**, 153–159 (2009).
18. Subach, O. M. et al. Conversion of red fluorescent protein into a bright blue probe. *Chem. Biol.* **15**, 1116–1124 (2008).
19. Shaner, N. C., Steinbach, P. A. & Tsien, R. Y. A guide to choosing fluorescent proteins. *Nat. Methods*. **2**, 905–909 (2005).
20. Stadler, E. et al. A versatile method for the determination of photochemical quantum yields via online UV-Vis spectroscopy. *Photochem. Photobiol Sci.* **17**, 660–669 (2018).
21. Kabsch, W. & Xds *Acta Crystallogr. D* **66**, 125–132 (2010).
22. The CCP4 suite. : programs for protein crystallography. *Acta Crystallogr. D*. **50**, 760–763 (1994).
23. Vagin, A. & Teplyakov, A. Molecular replacement with MOLREP. *Acta Crystallogr. D*. **66**, 22–25 (2010).
24. Emsley, P. & Cowtan, K. Coot: model-building tools for molecular graphics. *Acta Crystallogr. D*. **60**, 2126–2132 (2004).
25. Subach, O. M. et al. Slowly reducible genetically encoded green fluorescent indicator for in vivo and ex vivo visualization of hydrogen peroxide. *Int J. Mol. Sci* **20**, 3138-3162 (2019).
26. Chudakov, D. M. & Lukyanov, K. A. Use of green fluorescent protein (GFP) and its homologs for in vivo protein motility studies. *Biochem. (Mosc)*. **68**, 952–957 (2003).

Acknowledgements

The work was carried out within the state assignment of the National Research Center "Kurchatov Institute" to F.V.S. (developing and characterization of the PSmOrange3 protein), by the thematic plan of National Research Center Kurchatov Institute to V.R.S.(crystallization, data collection and structural studies), mammalian plasmids construction and transfection experiments were partially funded by RSF project number 24-74-10105, https://rscf.ru/en/project/24-74-10105/. This research was partially funded by National Science Foundation of China 32150015 to Y.Z.; by start-up funding from the Foundation of Westlake University, Westlake Laboratory of Life Sciences and Biomedicine, National Natural Science Foundation of China grant 32171093 and "Pioneer" and "Leading Goose" R&D Program of Zhejiang 2024SSYS0031 to K.D.P. The work was also supported by the Resource Centers department of the National Research Center Kurchatov Institute (imaging of bacterial cells and cultivation of mammalian cells). We thank Stavrini Papadaki and Xun Gao from Westlake Laboratory for verifying all plasmid sequences and depositing them to WeKwikGene. The authors acknowledge the support of the Omics Laboratory at Skolkovo Institute of Science and Technology for LC-MS/MS analysis.

Author contributions

O.M.S. developed the PSmOrange3 fluorescent protein, investigation, visualization. A.V.V. and Y.K.A. performed FPLC and purification of PSmOrange3 protein, investigation. O.M.S. and F.V.S. characterized PSmOrange3 in vitro, investigation, visualization. O.M.S., F.O., K.D.P., and F.V.S. characterized PSmOrange3 in mammalian cells, investigation, visualization. V.R.S., A.B. and V.B. crystallized PSmOrange3 and solved its structure, investigation, visualization. A.S.K., A.Y.N. and O.M.S. carried out mass spectrometry analysis. M.T., Y.Q., Y.Z., M.M.P., and A.S.M. performed PALM characterization and comparison of PSmOrange, PSmOrange2 and PSmOrange3, investigation, visualization. O.M.S., K.D.P., and F.V.S. analyzed and interpreted the data. O.M.S., K.D.P., and F.V.S. wrote the manuscript, writing – original draft. V.R.S., Y.Z., V.B., A.S.M., K.D.P. and F.V.S., funding acquisition. All authors reviewed the manuscript, writing – review and editing. All authors have read and agreed to the published version of the manuscript.

Declarations

Competing interests

The authors declare no competing interests.

Additional information

Supplementary Information The online version contains supplementary material available at https://doi.org/10.1038/s41598-025-23873-4.

Correspondence and requests for materials should be addressed to F.V.S.

Reprints and permissions information is available at www.nature.com/reprints.

Publisher's note Springer Nature remains neutral with regard to jurisdictional claims in published maps and institutional affiliations.